European Congress on Computational Methods
in Applied Sciences and Engineering (ECCOMAS 2012)
J. Eberhardsteiner et.al. (eds.)
Vienna, Austria, September 10-14, 2012

ANALYSIS AND APPLICATION OF SUITABLE CFD-BASED OPTIMIZATION STRATEGIES FOR HIGH-LIFT SYSTEM DESIGN

Pierluigi Iannelli[1], Jochen Wild[2], Mauro Minervino[3,1], Frederic Moens[4] and Michael Raets[5]

[1] CIRA - Italian Aerospace Research Centre, Aircrafts/Fluid Mechanics Unit, Fluid Dynamics Lab.
Via Maiorise, Capua, 81043, Italy
e-mail: p.iannelli@cira.it - m.minervino@cira.it

[2] DLR - German Aerospace Research Centre, Institute of Aerodynamics and Flow Technology
Lilienthalplatz 7, Braunschweig, 38108, Germany
e-mail: Jochen.Wild@dlr.de

[3] Piaggio Aero Industries S.p.A., P.H.T. - Piaggio High Technology Department
Via Campi Flegrei 34, Pozzuoli, 80078, Italy

[4] ONERA - The French Aerospace Lab., Applied Aerodynamics Department, Civil Aircraft Unit
Rue des Vertugadins 8, Meudon, 92190, France
e-mail: frederic.moens@onera.fr

[5] ASCO Industries N.V. – Engineering Department
Weiveldlaan 2, Zaventem, 1930, Belgium
e-mail: michael.raets@asco.be

Keywords: high-lift, design, optimization, natural laminar flow, multidisciplinary

Abstract. *The design of high-lift (HL) systems represents a challenging task within the aerospace community, due to its multidisciplinary, multi-objective and multi-point nature. Within the paper an additional difficulty is considered, consisting in the design of a HL system for a High Aspect Ratio Low Sweep (HARLS) wing, featuring Natural Laminar Flow (NLF) at transonic cruise conditions. In a first "analysis" phase a realistic optimization problem is defined and solved by adopting different approaches in terms of employed flow model, meshing strategies, geometry parameterization and optimization strategies. In a second "application" phase, the design of an optimal feasible HL system is developed for the HARLS-NLF wing, by considering a close coupling between 3D CFD-based optimization, kinematical layout studies and mechanical integration studies.*

1 INTRODUCTION

As well known, the design and optimization of High-Lift (HL) systems represents a challenging task for aircraft manufacturers, due to its multidisciplinary, multi-objective and multi-point nature. The design of HL devices typically involves the improvement of performances related to different flight phases, *e.g.* Take-Off (TO) and Landing (LDG). Normally, in each flight phase several performance indexes are to be improved or controlled at different flight conditions, and airworthiness requirements additionally pose both important boundaries to the design space and complicate the optimization problem formulation. Moreover, manufacturing constraints must be respected, as the designed shape must ensure enough structural stiffness to maintain the high aerodynamic loads occurring whereas, the external shape of the retracted wing must be compliant with the designated cruise clean wing shape. Finally, during the design phase the mechanical integration and kinematical reliability must be accounted for, in order to avoid unrealistic aerodynamic designs. All these features make the task of designing a HL system particularly difficult and often translate into stiff scenarios.

The DeSiReH project (Design, Simulation and Flight Reynolds Number testing for advanced High Lift Solutions) [1], funded by the European Commission in the 7th Framework Program, aims at improving the aerodynamics of HL systems by considering, in a coordinated approach, the development of both efficient numerical design strategies and measurement techniques for cryogenic wind tunnel conditions. It represents the follow up to the EUROLIFT I and II projects, wherein both numerical and experimental studies were mainly targeted towards validation of CFD tools for maximum lift prediction of increasingly complexity configurations up to flight Reynolds numbers. The target application of the DeSiReH project is the design of a realistic HL system for a High Aspect Ratio Low Sweep (HARLS) wing, featuring Natural Laminar Flow (NLF) at transonic cruise conditions.

Within this paper, an overview is given of the CFD-based optimization activities carried out in two phases of the DeSiReH project. In a first "analysis" phase (*i.e.,* Task 1.2), a realistic multi-objective/multi-point optimization problem is defined and solved by a group of partners adopting different approaches in terms of employed flow model, meshing techniques, geometry parameterization and optimization strategies. The results obtained are compared and efficiencies/deficiencies of the adopted approaches are highlighted. The experience gained in the first phase of the project is exploited in a second "application" phase (*i.e.,* Task 2.1), wherein the design of an optimal feasible HL system is developed for a HARLS-NLF wing. In this phase the design work is first concentrated on the 2D assessment of several candidate concepts, by considering CFD-based 2D optimization targeting lift maximization. At the same time, mechanical integration aspects are gradually developed and integrated into the explored HL concepts, leading afterwards to a refined constrained optimization of the 2D concepts. Based on 2D performance comparisons and integration aspects, the most promising concepts are down selected and a detailed 3D numerical optimization is carried out afterwards, for selected leading edge and trailing edge concepts. In this 3D phase the matured mechanical and structural constraint directives are included in the optimization loop. The solution of the 3D HL optimization problem is detailed and the final results obtained are described within the paper.

2 ANALYSIS OF HIGH-LIFT DESIGN STRATEGIES

Within the DeSiReH project, the work package 1 (WP1) is specifically dedicated to the analysis and improvement of HL aerodynamic design strategies. In Figure 1 it is shown the WP1 structure wherein Task 1.1 (T1.1) aims at defining efficient formulations of the HL optimization problem as a first step towards a reduction of design cycle time. Therein, identifi-

cation of appropriate target functions (including airworthiness requirements), of reduced number of design variables for shape parameterization and cost function parameter evaluation are investigated.

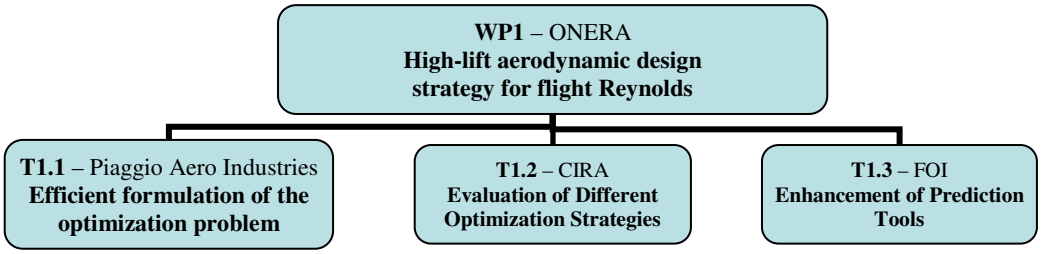

Figure 1: Work Breakdown Structure of the WP1 in the DeSiReH project.

In T1.2 the optimization of the full HL flight envelope is addressed, by considering a realistic design problem and different optimization approaches. Specifically, one aim of T1.2 is to compare different partners' optimization strategies in a 2D framework and to demonstrate the feasibility of a full 3D optimization approach by employing industrial standards (from CAD to CFD). Finally, in T1.3 the computational efficiency enhancement of CFD prediction tools is addressed. Detailed technical information on T1.3 activities can be found in [2][3], whereas in the following subsections only the activities related to T1.2 will be illustrated.

2.1 Description of the HL optimization problem for the assessment of design strategies

A common HL optimization problem was formulated in T1.2, whose starting point is the 3D full span slat and flap DLR-F11 (KH3Y) Wing-Body HL configuration of Figure 2, at both Take-Off (TO) and Landing (LDG) settings. A large experimental database is available for the KH3Y model from the former European project EUROLIFT. The 2D optimization work focused on the DV6 section (located in the middle of the outboard wing) where the 2D flow assumption is more reasonable. Both slat and flap shape changes were constrained by the red bounding boxes of Figure 2, which mimic manufacturing limitations [4]. As detailed in [4][5][6][8], the target of the optimization work was twofold: *i)* reduction of time-to-climb in the 2nd climb segment for TO, and *ii)* reduction of fuel burn in the final LDG approach phase. The bi-objective/multi-point optimization problem, entirely formulated in a 3D framework, is summarized in Figure 3. The analyses in [4] show that the proposed optimization mostly reduces to a drag reduction problem at constant lift and fixed angle of attack at both TO and LDG. The design points (DP) flow conditions were extracted from the KH3Y experimental polars (*i.e.*, $C_{L\max}$) and according to the EASA CS-25 regulations on characteristic speeds. Additional design points (DP2) were included to guarantee that the optimized configuration provides at least the same lift level of the baseline in the full flight envelope. The drag inequality at LDG was derived according to airworthiness requirements on both minimum thrust levels in the final approach phase and minimum climb gradient in the go-around phase. The constants in Figure 3 were derived according to the EASA CS-25 regulations and from statistical values of both thrust to weight ratio and thrust at approach idle. Finally, the pitching moment coefficient was allowed to increase by no more than 15% at all DPs with respect to the initial configuration. One peculiarity of the proposed design problem is that the two objectives are correlated by means of the sole slat/flap shape variables, whereas setting variables affect either the TO or the LDG objective only. Differently from other partners, Airbus-Military (AI-M) replaced the original LDG objective (min C_D) with lift improvement (F_{LDG}= $-C_L|_{\text{LDG-DP1}}$), as it represents a typical target in military applications. Moreover, in order to re-

duce the computational efforts, the 3D optimization was restricted to the TO problem and only the 3D flap optimization (shape and setting) was targeted.

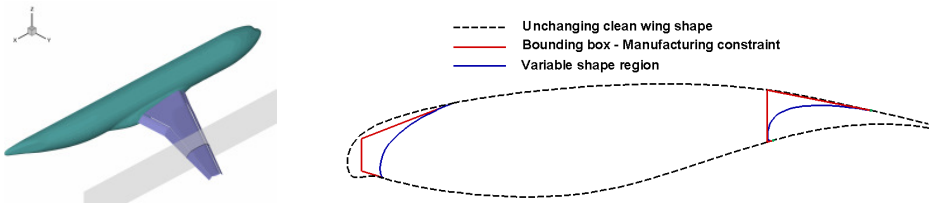

Figure 2: KH3Y full span slat/flap model and DV6 section location (left). Retracted streamwise 2D cut (right).

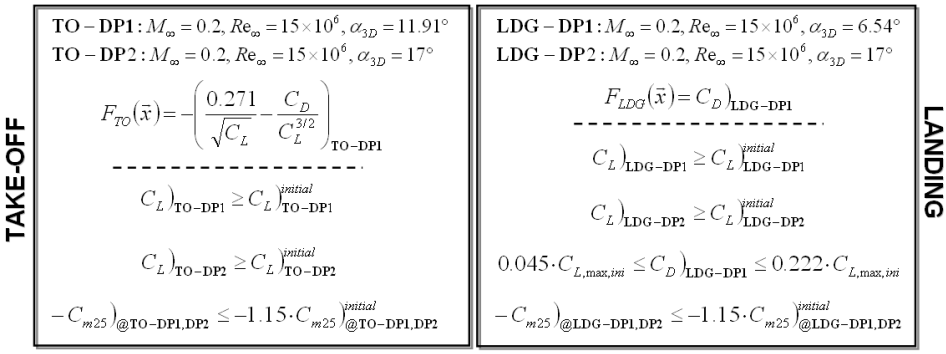

Figure 3: Bi-objective/multi-point optimization problem formulation.

2.2 Summary of the employed optimization tools

A specific procedure based on the infinite swept wing theory and additional corrections has been developed over the years [4][6][7] to correlate the 2D CFD predictions and the real 3D aerodynamic performance. As suggested in [7], a CFD tools calibration phase has been firstly performed to avoid a large spreading of partners' results at the end of their optimization work. Before any optimization work each partner has assessed its CFD setup (*e.g.*, solver settings, meshing strategy/density, turbulence model, 2D angle of attack, etc.) by comparison with the available experimental data. Table 1 summarizes the calibrated partners' CFD tools and their relevant settings, whereas in Figure 4 the calibrated 2D and 3D partners' predictions show a good agreement with the experimental data and a limited scatter of results. As shown, different meshing/CFD approaches (*i.e.*, multiblock structured/hybrid/Chimera) have been used, as well as both commercial and in-house developed software. In Table 2 is presented a summary of partners' employed shape parameterization, optimization approach, number of Design Variables (DVs) and optimization algorithms. As shown, a group of 2D partners such as Airbus-Germany (AI-D), ONERA and Airbus-Military (AI-M) simplified the problem into decoupled sequential/single-objective sub-problems, characterized by a reduced design space.

Dimension	Partner	Solver	Grid Generator	Grid Type	Grid size	Turb. model
2D	AI-D	TAU	In-house CENTAUR	2D Hybrid	135 Knodes	k-ω MSST
2D	UNIPD	ANSYS Fluent	ANSYS Gambit	2D Structured	220 Kcells	k- ω SST
2D	CIRA	ZEN	ANSYS ICEMCFD/Hexa	2D Structured	100 Kcells	k- ω TNT
2D	DLR	FLOWer	In-house MEGACADS	2D Structured	90 Kcells	SA (Edwards)
2.5D	ONERA	elsA	In-house MESH 3D	2.5D Chimera	88.5 Kcells	SA
2D	AI-M	ANSYS CFX	ANSYS ICEMCFD/Hexa	2D Structured	100 Kcells	k- ω MSST
3D	AI-M	ANSYS CFX	ANSYS ICEMCFD/Hexa	3D Structured	2.5 Mcells	k- ω MSST
3D	PAI	Metacomp CFD++	ANSYS ICEMCFD/Hexa	3D Structured	2.8 Mcells	k- ω SST

Table 1: Calibrated CFD setup used by partners in the optimization work (PAI = Piaggio Aero Industries).

The most simplified case is represented by the AI-D approach, wherein the two objectives were made independent by considering only slat/flap setting DVs and no shape optimization. Differently, ONERA and AI-M first performed LDG optimization including shape variables and then focused on TO setting-only optimization with a frozen (optimal) shape. Specifically, AI-M considered a "physics-based" approach characterized by sequential optimizations of small size sub-problems. Herein, each flow mechanism limiting the C_L increase is controlled with few DVs (e.g., flap separation controlled by flap position, off-surface separation controlled by slat position, etc.) and suitable "physical" sensors are used to detect adverse flow mechanisms [6]. As reported in [6][8], ONERA also attempted a "by element" sequential optimization, wherein first the slat is optimized at TO and LDG with the flap in a reference position and then the flap is optimized at TO and LDG with a frozen "optimal" slat shape/position. Such approach revealed to be ineffective for the current drag-based optimization, though it is known to work in lift-based optimizations. In the DLR approach a single-objective/multi-point optimization is considered, wherein the TO/LDG objectives have been cumulated into a single one. In this case the design space size is not reduced but the problem is re-formulated as a single-objective optimization.

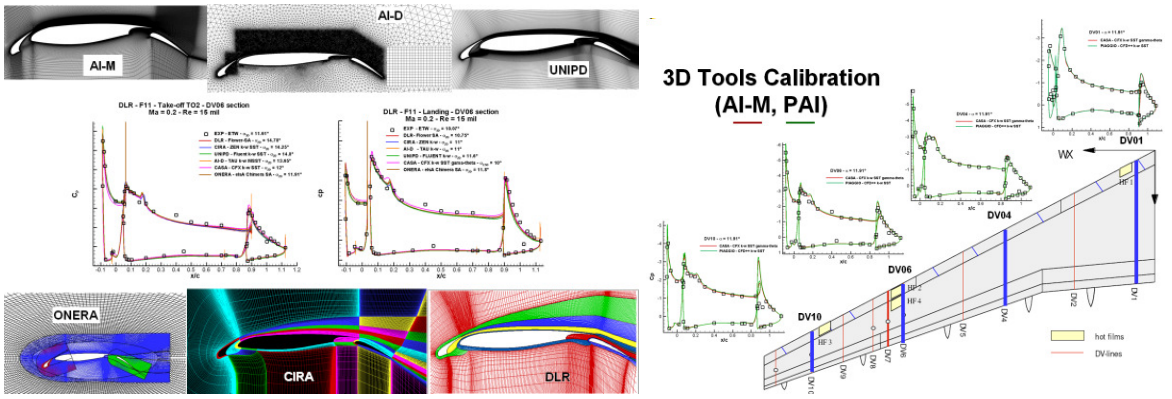

Figure 4: 2D partners' calibration and meshing strategies (left) and 3D calibration results (right).

Finally, UNIPD and CIRA performed the original bi-objective optimization problem using 22 and 28 DVs, respectively, and similar evolutionary algorithms. Regarding the 3D optimization, Table 2 shows that both partners employed a Genetic Algorithm though using different strategies. In fact, while AI-M performed a pure setting optimization, PAI included the flap shape optimization where 4 DVs control the flap shape at the kink section and the modifications are linearly extended along the wingspan [5]. It is worth remarking that most of the partners employed parallel resources to carry out the optimization work.

Dimension	Partner	Shape parameterization (DV)	Opt. approach & DVs	Opt. Algorithm
2D	AI-D	No shape optimization	Sequential: TO(6) → LDG(6)	Best engineering practise
2.5D	ONERA	Bézier curves (14)	Sequential: LDG(20) → TO(6)	Covariance Matrix Adaptation Evolution Strategy
2D	AI-M	Overposition of modes (3)	Sequential: LDG(9)→ TO(6)	Nelder Mead Simplex+GA → GA
2D	DLR	Free-form deformation (5)	Cumulated Obj: TO+LDG (17)	Rowan's subplex
2D	UNIPD	Bézier curves (10)	Bi-Obj: TO&LDG (22)	GA + Gradient on Surrogate Model
2D	CIRA	Overposition of modes (16)	Bi-Obj: TO&LDG (28)	Genetic algorithm (GA)
3D-TO	AI-M	No shape optimization	Single Obj: TO(6)	Genetic algorithm
3D-TO	PAI	Conic curves + B-splines (4)	Single Obj: TO(11)	Genetic algorithm

Table 2: Summary of shape parameterizations, optimization approaches, number of design variables (DVs) and optimization algorithms employed by partners.

2.3 Optimization results

A detailed analysis of optimization results is given in [6] and only the major outcomes will be summarized herein. Three "evaluators" have been appointed (AI-D/ONERA/UNIPD), having the role of re-evaluating all 2D optimized geometries to verify the declared partners' performance improvements. According to the considered drag-reduction problem a careful treatment of different lift levels was needed to avoid mystifications of the real improvements achieved. To this aim, the cross-checking of performance is presented in Figure 5 for an equal C_L level (C_L=$C_{L,baseline}$). In Figure 5 the partners' optimized configurations are represented on the x-axis whereas the objective function variations (%) calculated by the evaluators are indicated with blue/red/green bars, respectively. An arithmetic average (yellow bars) is also plotted to filter the individual evaluators' responses and, for each partner, it is briefly indicated the strategy used and the number of individuals explored by the optimizing strategy.

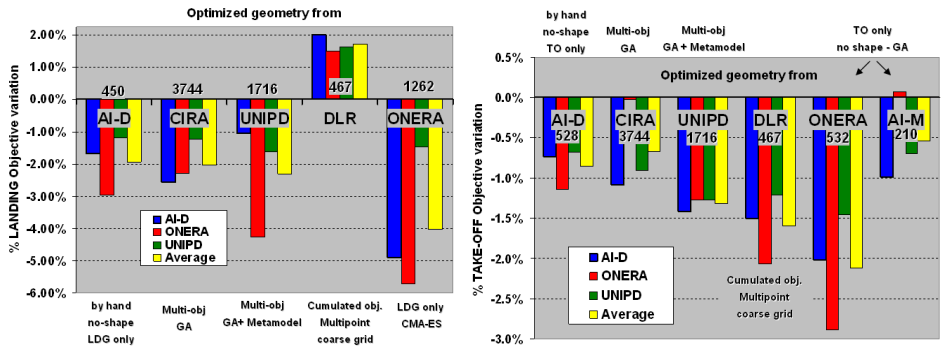

Figure 5: Cross-check of partners' 2D optimized geometries (LDG-left and TO-right) at constant lift.

It is worth saying that some partners performing post-processing of evolutionary optimization data, have found that the TO and LDG objectives are very weakly coupled in the proposed optimization problem. This was mainly due to the TO objective function, which is very poorly sensitive to slat/flap shape changes. Such analysis was confirmed by both CIRA and UNIPD Pareto fronts shown in Figure 6, having the shape of a very steep curve or "L-shaped" curve, indicating a tendency towards a unique solution of the problem, corresponding to optimal shape/settings at LDG and optimal TO settings (with an optimized LDG shape).

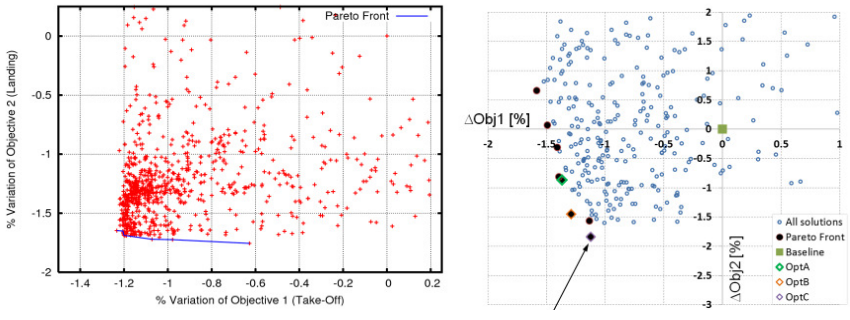

Figure 6: CIRA (left) and UNIPD (right) Pareto fronts.

In the following considerations the AI-D improvements/efforts (obtained with standard industrial procedures based on "by hand" parametric studies and high human interaction) can be considered as a reference level to assess the capabilities of automatic optimization tools. As shown, DLR-LDG configuration (Figure 5, left) is unanimously evaluated as worse than the initial one due to a coarse grid employed in optimization (22.5 Kcells vs. 90 Kcells used in

calibration). Such mesh density, thought inadequate for LDG optimization, was successfully employed at TO (Figure 5, right) where the DLR configuration improvement is 1.5% on average. CIRA and UNIPD obtained similar improvements using comparable approaches (bi-objective GA-based opt., large number of DVs). Specifically, UNIPD strategy shows slightly better performance over CIRA, likely due to the employed local search, gradient-based algorithm working on the Neural-Network Metamodel, which enhanced the global GA evolution rate. While CIRA/UNIPD results show little differences at LDG compared to AI-D, UNIPD improvements at TO are doubled compared to AI-D. On the other hand, ONERA worked with a reduced design space (especially at LDG) due to the applied decoupling and employed an (advanced) evolutionary approach as CIRA/UNIPD. Thanks to the reduced problem(s) size, the design space was more widely explored in each of the single-objective optimizations performed, thus providing larger improvements. This likely explains the best performance obtained by ONERA for both objectives considered. It is worth noting that direct comparison of AI-D vs. ONERA results at LDG show potentials of automatic optimization capabilities. Finally, in Figure 7 (left) the cross-checked performance of the AI-M (C_L-optimized) geometry is shown, confirming the achieved lift performance improvement obtained by means of only 101 evaluations. It is worth remarking that the poor performance of AI-M configuration at TO (obtained with a similar approach as ONERA) could be justified by the few evolutions of the GA algorithm considered. For the 3D optimization, only PAI results will be summarized for the sake of brevity, the AI-M results being not substantially different. As shown in Figure 7 (right) the 3D GA-optimization required approximately 1000 individuals evaluation (*i.e.*, 2000 CFD runs) to achieve a 0.4% improvement on the TO objective. The elapsed time for one CFD run was about 20 minutes on a 72 cores cluster, whereas one individual evaluation took approximately 50 minutes and in total 50K hours (35 days) have been spent for the optimization, thought without human interaction in between. In Figure 7 (right) it is shown that the 3D drag reduction at TO was obtained by increasing the flap load and decreasing the main wing load, with a consequent reduction of the main wing wake [5].

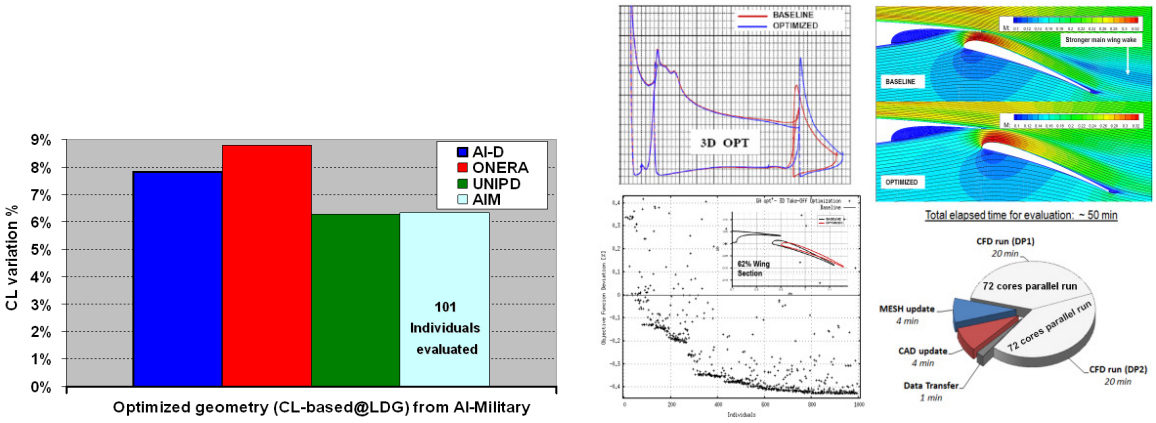

Figure 7 Cross-check of AI-M lift-based optimized geometry at LDG (left), PAI 3D optimization results (right).

2.4 Conclusions and lessons learned on the assessment of HL design strategies

Due to the heterogeneous set of approaches employed and to the specific problem considered, exhibiting quite flat objective functions, it is not possible to draw definitive conclusions on the best optimization strategy to employ in HL optimization. Nevertheless, the experience gained was useful to provide the following general guidelines for HL design and suggested areas for future investigations:

- For the same decoupled approach, the automatic ONERA optimization provided double improvements compared to the AI-D approach based on current industrial standards. This indicates that the introduction in industry of automatic optimization should be more and more pursued, as it would allow for interesting margins of performance improvements. Nevertheless, other partners' results have shown that automatic optimizations not always produce clear improvements over the industrial approach. This happens especially when the design space is not adequately explored (either because the design space is too wide or because the optimization is stopped prematurely).
- Observation of CIRA/UNIPD/ONERA-LDG optimizations indicates that the usage of a high number of DVs requires a large number of evolutions to achieve significant improvements in evolutionary approaches. In this context, comparison of CIRA vs. UNIPD performance indicates that usage of surrogate models helps enhancing convergence. Moreover, ONERA-LDG optimization results (using a comparable number of DVs as CIRA/UNIPD) indicate a potential superiority of the employed Covariance Matrix Adaptation Evolution Strategy algorithm in comparison to classical evolutionary approaches.
- The usage of decoupling/sequential strategies (allowing a reduced design spaces) is highly recommended. However, not all the sequential strategies are effective. As mentioned above, the "by element" decoupling considered by ONERA resulted to be unreliable for the current drag-based problem, whereas the "by configuration" sequence shown herein demonstrated to be very useful. This indicates that applicability of sequential strategies must be assessed *a-priori* by preliminary analyses or pre-knowledge of the optimization problem.
- AI-M (LDG) physics-driven optimization, being based on a very small number of DVs proven to be very powerful and cost-effective. As expected, the introduction of engineering knowledge allows efficient formulation/solution of the problem and it is always suggested whenever possible.
- The DLR experience indicates that strategies based on approximate fitness function evaluation (*i.e.*, coarse grid) are to be carefully employed in HL numerical optimization and that preliminary assessments are needed to setup a reliable strategy.
- The employment of a full automatic 3D HL optimization chain based on currently available industrial tools looks feasible nowadays. As shown, it requires large but not prohibitive computational resources and based on the above 2D outcomes it could provide interesting margins of improvements with respect to the parametric industrial approach.
- In cooperative optimization activities, in order to further reduce the scatter of partners' improvements quantification (as shown in Figure 5), it is suggested to perform the CFD codes calibration (on the initial configuration) by considering also lift and drag coefficients rather than only matching the experimental pressure distributions as considered herein.

3 DESIGN OF A NLF-WING COMPATIBLE HIGH-LIFT SYSTEM

Based on the experience gained during the assessment of optimization strategies, these methods are in a second step applied to a very challenging design task. The application shall demonstrate the benefits of using optimization based design methods for real world applications and their special strength for design tasks when leaving known design spaces. Figure 8 depicts the structure of the Work Package 2, where in task 2.1 the design of the HL system is performed. Task 2.2 addresses high-fidelity analyses of the design including all major impacts expected to show up during the wind tunnel verification in the European Transonic Wind Tunnel facility (ETW). Finally, task 2.3 will assess the quality of the predictions by compar-

ing the obtained wind tunnel data with the CFD based predictions. Within the design task first suitable concepts are identified by using the same wing section design methodology as it was used and evaluated in the two-dimensional optimization framework reported earlier. In addition to the purely aerodynamics driven optimization method, feasibility of the designed HL system is a major intention of the performed design work within this work package.

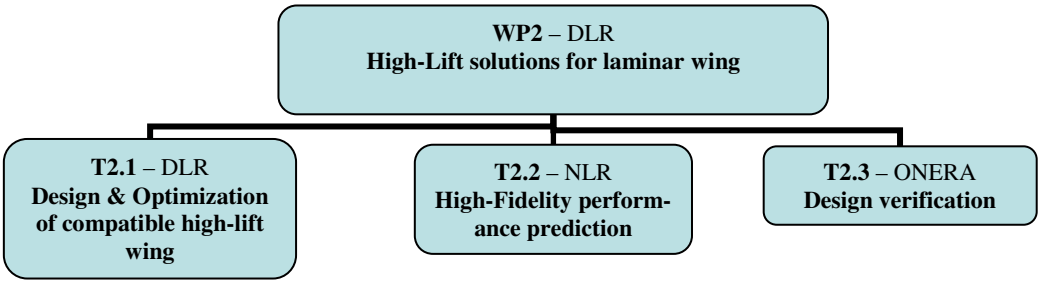

Figure 8: Breakdown of the work package assigned to the design of the laminar wing compatible high-lift system.

Especially, leading edge devices stored into a NLF wing pose larger difficulties due to the relatively limited space available. In order to achieve this goal in parallel to the design work, the concepts investigated were assessed in terms of suitable kinematics and their mechanical integration. Conflicts arising from this view were used in refinements of the designs, especially by posing the necessary geometric constraints. Finally the complete high-lift system for the 3D wing was designed making again use of the experience gained in the first work package concerning aerodynamic 3D high-lift system optimization.

3.1 Selection of NLF wing compatible high-lift systems

Prior to any design work, the type of HL system to be adapted to the wing has to be defined. The key parameter to help for the selection is the required level of maximum lift in landing conditions, which depends on the aircraft weight and wing area. For the current configuration, the maximum lift of the clean wing configuration has to be increased at least of $\Delta C_{L,\max}=1.25$ for landing. The use of a trailing-edge system is therefore mandatory, but a classical Fowler single slotted flap should generate sufficient lift. Even a double slotted flap or flaps that incorporate spoiler droop seem feasible and well known solutions.

However, the use of a trailing-edge device alone will necessarily lead to an unacceptable decrease in $\alpha(C_{L,\max})$. Increasing this angle is possible only through the use of a leading-edge device [9], though this system must be compatible with a NLF wing at cruise conditions.

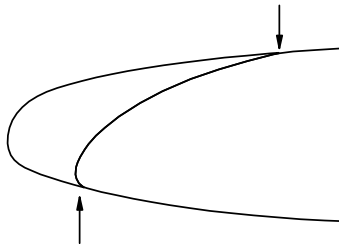

Figure 9 : Incompatibility of standard leading-edge slat with NLF technology.

Therefore, standard leading slat are not acceptable as there will be manufacturing irregularities (steps or gaps) at the junction with the main wing that will alter the laminar behavior in cruise (Figure 9). The first part of the selection is to compare several concepts for leading-

edge devices that are compatible with NLF technology based on aerodynamic performance only. Then, integration aspects will be considered in the final optimization process.

3.2 Evaluation of individual leading-edge devices

Figure 10 presents the different leading-edge devices concepts evaluated. The shape of the clean wing section is superimposed in red for reference.

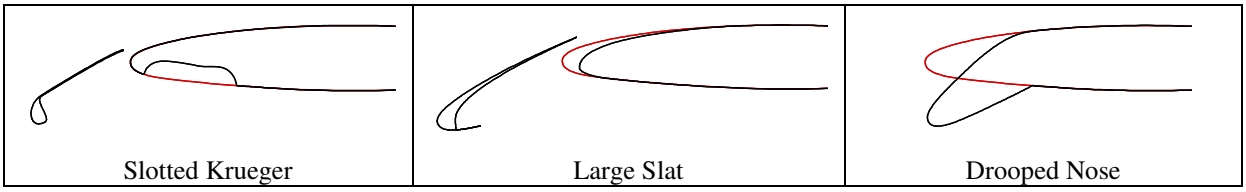

Figure 10 : Leading-edge devices concepts evaluated.

The main characteristics of the three concepts investigated are summed-up hereafter:

- The Krueger device is generally considered as a good compromise to ensure a good performance level at low-speed conditions with only a possible loss of laminar flow only on the lower side at cruise conditions. In addition, the use of a slot gap improves dramatically the performance compared to a sealed configuration [9][10].
- Another concept considered is a slat with a very long chord (about 30%). The problems of surface irregularities at wing junction observed for standard slats still remain, though it will occur at a downstream location on the upper surface where a thicker boundary layer transition may be less affected by surface discontinuities.
- Finally, a drooped nose is also considered as it is the only concept that makes possible to keep the laminar flow at cruise conditions on both surfaces.

Each device has been studied separately from trailing edge devices, in order to assess its potential contribution to the final performance when both leading/trailing-edge devices are combined. Let us remind that at the end of such design phase these configurations did not correspond to a real optimized one, as no constraints of the system integration were included. Therefore, computations carried out in this part have to be considered as a rough assessment of the potentials of each device, and several partners were involved in this preliminary design study. In order to make a fair comparison between concepts, some cross-check computations have been made by ONERA using the same code at two important steps of the selection: for the evaluation of individual concepts and for the evaluation of pre-optimized systems.

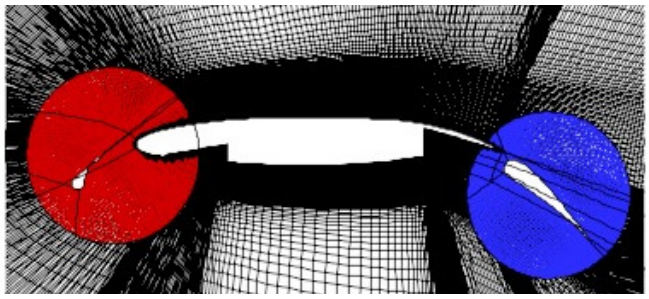

Figure 11 : Example of chimera grid used.

In order to facilitate the grid generation process for all the configurations to be evaluated, the chimera technique has been used (Figure 11). All the evaluations have been carried out in

2.5D mode, by assuming a leading-edge sweep of 18° and by considering the following flow conditions : M_0=0.20 at z=0 ft, leading to a local Reynolds number of $13 \cdot 10^6$ for the wing section considered. The Spalart-Allmaras turbulence model has been used. Figure 12 compares the computed aerodynamic performance for the three concepts considered in term of $C_L(\alpha)$ and $C_L(C_D)$ curves (2.5D results). First of all, it is interesting to note that the required level of C_{Lmax} is more or less reached by every concept individually (except for the drooped nose), and we can clearly see that the use of a slotted device is much more efficient than the use of a drooped nose in term of C_{Lmax} and $\alpha(C_{Lmax})$. In addition, they lead to an increase of the slope of the $C_L(\alpha)$ curve. Then, in a second view, the Krueger seems more interesting that a Large Slat, because:

- Both configurations have nearly the same performance;
- The Krueger configuration produces less drag;
- There is no gap on the upper surface;
- The Krueger produces an "insect shielding" effect for the clean airfoil leading-edge.

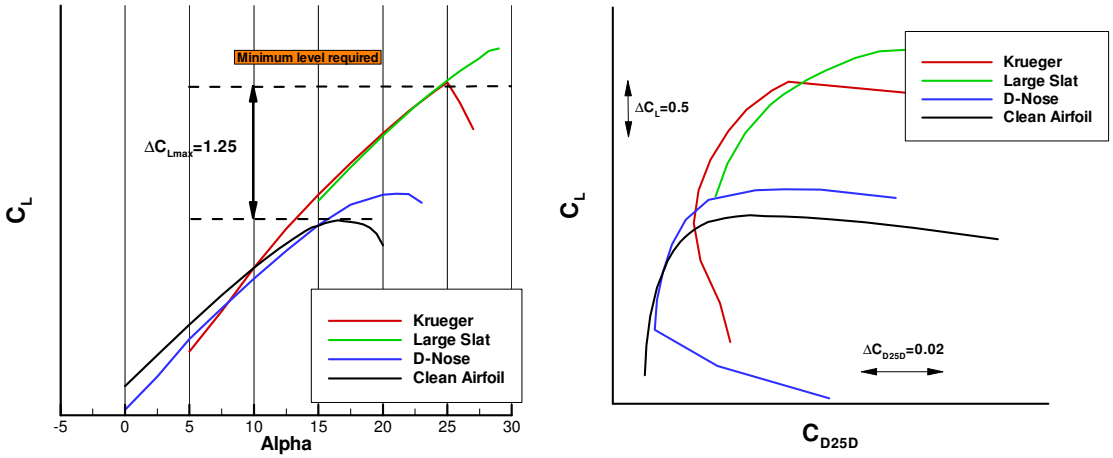

Figure 12 : Individual concepts – 2.5D aerodynamic performances (M_0=0.20, Re_C=12.9·10^6).

Considering the stall behavior of the different leading-edge concepts, Figure 13 compares the evolution of the minimum pressure level at leading-edge for the different elements of the three concepts.

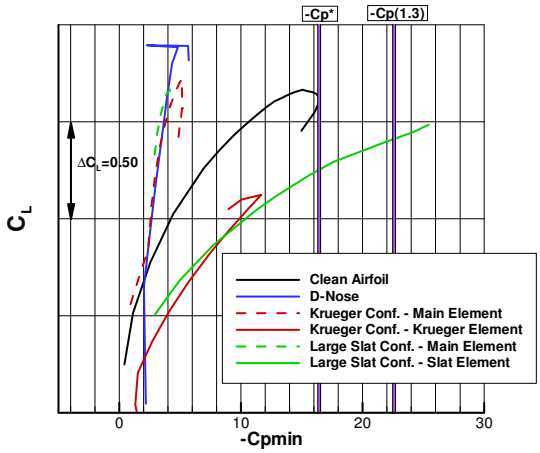

Figure 13 : Stall behavior for leading-edge devices (2.5D computations).

Two pressure coefficient levels are indicated in Figure 13, corresponding to a freestream Mach number of M_0=0.20 and local isentropic Mach numbers of 1 (C_P*) and 1.3 ($C_{P(1.3)}$), respectively. For the drooped nose considered, there is a trailing-edge separation stall, whereas for slotted devices (the highest level of local velocity is on the device) the stall is driven by leading-edge stall of the Krueger/slat. However, the Large Slat concept is more sensitive than the Krueger concept: for the same lift, there is a higher level of minimum pressure peak at high α for the Large Slat than for the Krueger. For the Krueger concept, it can be noted that the gradient of the minimum pressure peak with C_L on the main element is similar to the one observed for the clean airfoil (same geometry), and that the minimum pressure peak is located on the Krueger device, not on the main element. For 3D integration, it seems easier to control the wing stall by the use of slotted Krueger, which span-wise settings can be adapted independently. Based on this evaluation phase, it was decided to consider a HL system with a slotted Krueger element as leading-edge device.

3.3 Evaluation of pre-optimized high-lift systems

Once the high-lift system devices have been down-selected, some preliminary optimizations have been carried out by different partners. At this stage, some design constraints have been introduced. Figure 14 presents the different configurations issued from this study. The first one (Design 1) it has been designed by adopting standard industrial design methodologies and considers a relatively small Krueger as leading-edge device and a classical Fowler flap at the trailing-edge. For the two other configurations, a numerical optimization process has been used and a spoiler droop at the wing trailing-edge has been considered for improved lifting performance. Note that the spoiler parameters have been considered as design variables in the optimization. Design 2 considered only maximum lift to be optimized, whereas a multi-point optimization was considered for Design 3, taking into account some minimum performance levels at lower angles of attack which still represent realistic flight conditions.

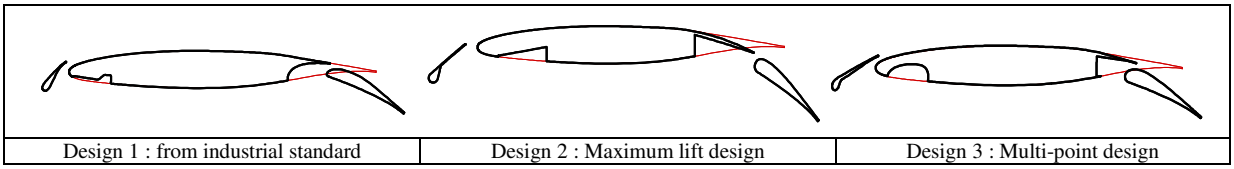

Design 1 : from industrial standard	Design 2 : Maximum lift design	Design 3 : Multi-point design

Figure 14 : Pre-optimized high-lift configurations.

Similarly to the concept evaluation phase, a cross-checking exercise has been carried out by ONERA with a single code in order to compare solutions issued from different partners. Figure 15 compares the estimated 3D performance of the wing equipped with the different pre-optimized configurations. First of all, all the configurations meet the target in terms of maximum lift level. The Design 2 configuration generates the highest maximum lift coefficient, but a separation occurs on the flap for angles of attack below 14°, which leads to a significant loss of lift compared to other designs. Comparison between Design 2 and Design 3 shows the necessity of a multi-point optimization in the design process in order to have good performance on the complete $C_L(\alpha)$ curve, not only close to maximum lift. Considering the $C_L(C_D)$ polar, the Design 1 and Design 3 configurations can be considered as equivalent. The main difference between the different designs is on the computed $\alpha(C_{Lmax})$ and the stall process. For the Design 1 and Design 2 configurations, there is a smooth decrease in lift after the maximum lift, whereas the stall is more abrupt for Design 3. Let us remind that these 3D predicted values were derived from the computed characteristics of a wing section, according to the 2D->3D prediction procedure developed and used in §2. The real 3D wing stall behavior

will probably be different (simply because the stall onset could occur at another wing section). Finally, it is worth noting that in all the configurations a recirculating region is found at the wing lower surface due to the Krueger cavity. This separation has a negligible impact on the overall performance though it could lead to noise sources.

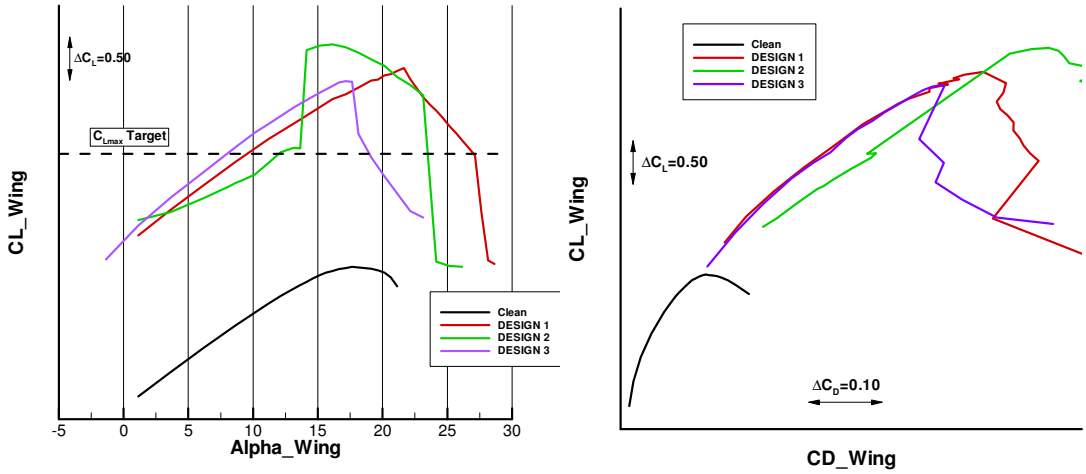

Figure 15 : Estimated 3D performance for the pre-optimized configurations.

For the final 3D numerical design phase, the Design 3 configuration has been considered as the baseline to be optimized, by taking into account integration constraints, including structural and kinematical aspects. On the other hand, the Design 1 configuration has been kept as the reference based on industry standards and it will be used for comparison purposes in future experimental activities.

3.4 High-Lift system kinematics solutions

As already mentioned, the mechanical integration feasibility is a core requirement for the design of HL systems. The selected trailing edge device concept is seen mature and therefore no distinct studies have been performed on it. Although a few transport aircraft already operate Krueger devices at the leading edge, the kinematics solution is not as mature. Especially, the Krueger device proposed for the DESIREH project is characterized by a significant gap to the main wing. Thanks to this, the Krueger is positioned towards the wing more like a slat device, which makes it necessary to reevaluate corresponding kinematics solutions.

Based on the 2D wing section designs used during the selection of the leading edge device, several concepts of actuation/kinematics were studied. Many concepts, mainly based on existing patents (US4262868, US4189120, US5158252, US3910530), were considered but in the end only two were selected for additional studies. Most of the rejected concepts did neither match the aero requirements nor the mechanism space allocation. Two concepts did not match the actual requirements perfectly either, but were the most promising for a workable solution. At the end a mechanism derived from the B757 HLFC (Hybrid Laminar Flow Control) experiment [10] was selected. First, only the actuation and the Krueger panel shape were used as a base for the design of a workable solution. The main characteristic of this concept is that, when deployed (low-speed regime), the ‘gooseneck’ link goes through an opening in the leading edge which is closed by an extension of the Krueger panel on this specific area in retracted configuration (cruise phase). The opening allows the linkage to extend further and hence also the (Krueger flap) panel, which is required in case of a vented Krueger flap device.

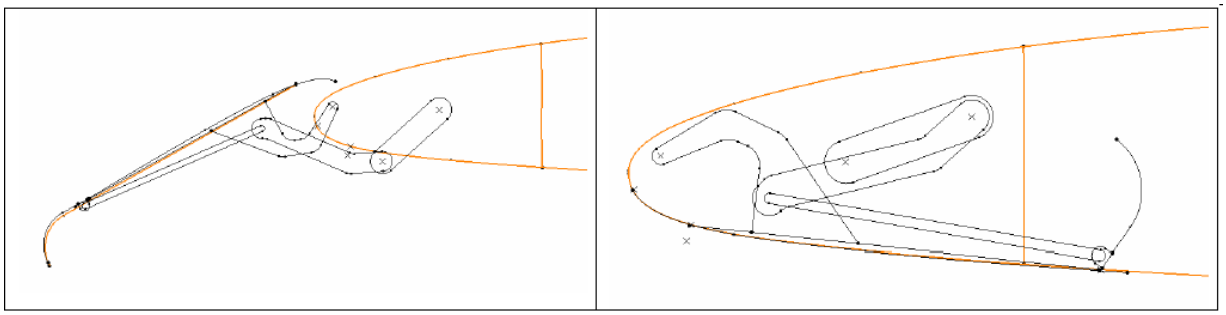

Figure 16: Krueger device B757HLFC Experiment Based Concept.

The main benefit of the concept is that it complies with the aero requirements. Also, the mechanism could fit in the allocated space even if the Bull Nose and Krueger panel with the first version of the Krueger design would go beyond the Front Spar, as depicted in Figure 16.

Another major concern is on the position of the rotation center point which is closely related to the position of the panel when extended. Figure 17 shows the confined space available at the station located closest to the design section at 60% wingspan. The Krueger flap in extended position is drawn in purple. The green lines reflect the stowed/retracted position with the bull nose folded 90° clockwise. The white sketch represents the most critical transit position in which the deploying/extending Krueger panel is placed in a 90° position compared to the free stream and is thus loaded with a purely horizontal drag force. A preliminary sizing of the actuation mechanism was performed based on initial CFD calculations. The red dotted line borders a zone with a 40 mm clearance from the outer wing skin. The hinge point should preferably be located in this zone to give space for bearings of adequate size. The orange circle on Figure 17 represents a rough estimation of the relatively large Geared Rotary Actuator (GRA) diameter. A provisional calculation of the load distribution on the mechanical actuation system during operational conditions reveals a maximum reaction torque. Taking into account failure/skew modes leads to a UTLS (Upper Torque Limiter Setting) around 500-600 daNm. By using an empirical relation function between UTLS and the diameter of the GRA, this UTLS requirement results in a required GRA diameter of approximately 120-150mm.

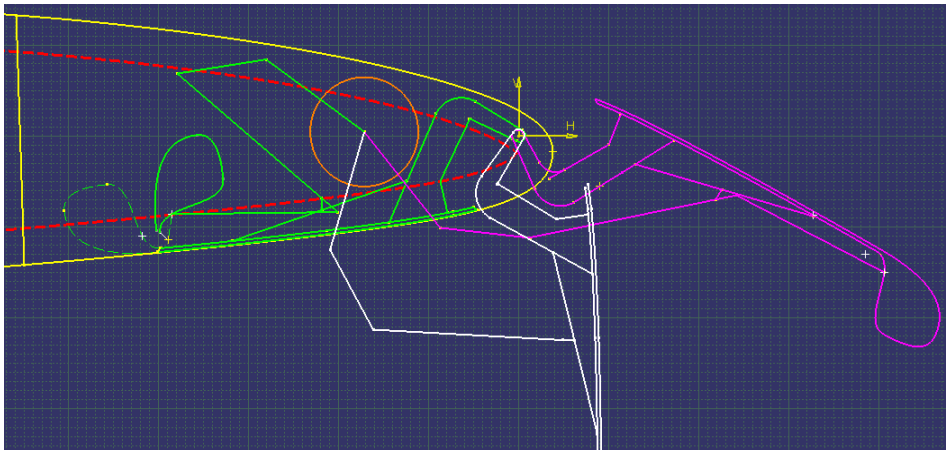

Figure 17: Sketch of actuation concept for section close to design station at 60% wing span.

The first aerodynamically driven designs of the Krueger itself showed up as very thin plate structures that would not be suitable. Again, based on the running CFD analysis during the concept design the aerodynamic loads were used to size the panel in terms of stiffness. In order to obtain a more realistically stiffened Krueger panel, it was proposed to add stiffeners

and ribs to the pressure side of the panel. This profile thickening is tapered towards the trailing edge. Adding a back skin to the panel will also increase the stiffness and will bring the deformations to a more acceptable order of magnitude. Such a stiffened Krueger panel can be seen in Figure 18.

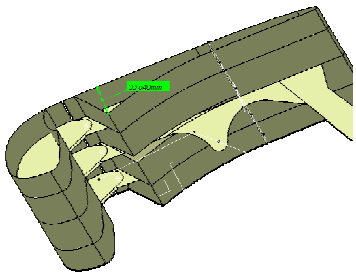

Figure 18: Stiffened Krueger flap panel.

The constraints arising from the mechanical integration assessment were fed back into the design process and according to it a mechanical feasible actuation system was achieved for the folding bull-nose Krueger based on the modified B757HLFC concept, as shown in Figure 19.

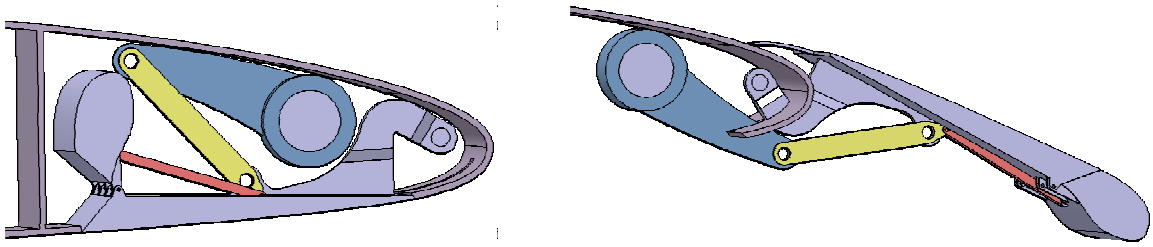

Figure 19: 3D DMU of sized actuation system based on updated folding bull-nose Krueger design (des.station).

3.5 3D CFD-based optimization of NLF-compatible High-Lift system

The optimization work shown herein was carried out by PAI by using the optimization chain developed in T1.2 and described in §2, made up of the CIRA in-house developed genetic algorithm software and the PAI industrial CAE tools (*i.e.*, CATIA v5 CAD modeler, ANSYS-ICEMCFD mesh generator and Metacomp Tech. CFD++ solver). The HL system was required to enable an approach speed of the reference aircraft (130 pax, MLW=67 t) of V_{REF}=135 KCAS. The optimization aimed at improving the aerodynamic efficiency at landing approach conditions (Design Point 2, Table 3), while preserving attached flow on the suction side over the complete speed range flown with flap extended, and providing a $C_{L,max}$ above a specified target (Design Point 0). The attached flow requirement is weighted into the design by the introduction of an additional objective, i.e. C_L maximization at flight speed V_{FE^*} ($V_{FE^*}=1.6 \cdot V_S$) close to V_{FE} (maximum allowed flight speed with flap extended – Design Point 1).

Design Pt.	Altitude	Speed	M	Re	Angle of Attack	Target
DP0	Sea Level, ISA	$V_S=V_{REF}/1.23$=109.8 KCAS	0.166	$14 \cdot 10^6$	$\alpha(C_{L,MAX})$	$C_{L,MAX} > 2.54$
DP1	Sea Level, ISA	$V_{FE^*}=1.3 \cdot V_{REF}$=175.5 KCAS	0.266	$22 \cdot 10^6$	$\alpha_{base}(C_L=1.00)$	$\max(C_L)$
DP2	Sea Level, ISA	V_{REF}=135 KCAS	0.2	$17 \cdot 10^6$	$\alpha_{base}(C_L=1.68)$	$\max(E^2 C_L)$

Table 3: Aerodynamic Targets for HLS optimization (lift coefficients refer to the wing alone).

A general planform arrangement for the HL system, including front and rear spar limitations to the design, was provided by AI-D together with the reference clean wing shape. This was used as an input to develop from scratch a fully parametric 3D CAD model of the HL

system, using a total of 18 Design Variables (9 shape + 9 setting). Both the Krueger and the trailing-edge flap devices were modeled using two design sections (root and tip) with simplified shape definition (conical, circular and spline curves) as shown in Figure 20 and described in §2 and [5]. The Fowler flap hinge line position and device deflection were free to be modified by the optimizer (chords, shroud length and lip thickness unchanged), while for the Krueger device the tip hinge point was frozen at its baseline position and modifications of the Krueger tip chord were allowed. Downward spoiler deflections up to 8° provided an additional degree of freedom to increase the wing curvature (Figure 21).

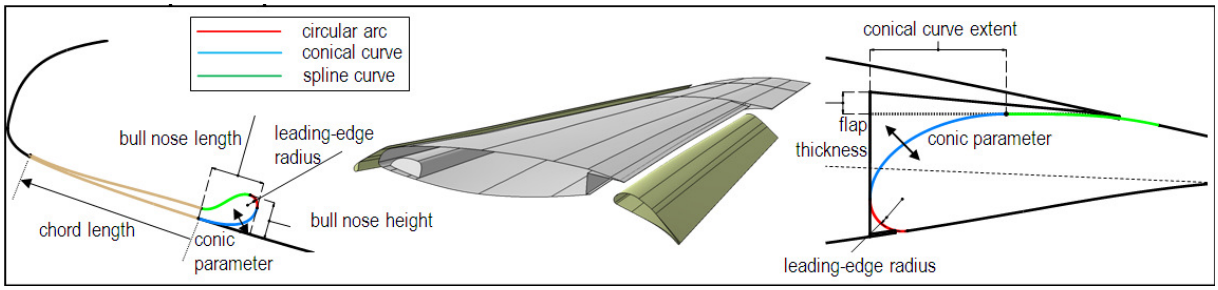

Figure 20: Parametric CAD shape modifications (5 DVs for Krueger section shape + 4 DVs for the t.e. flap).

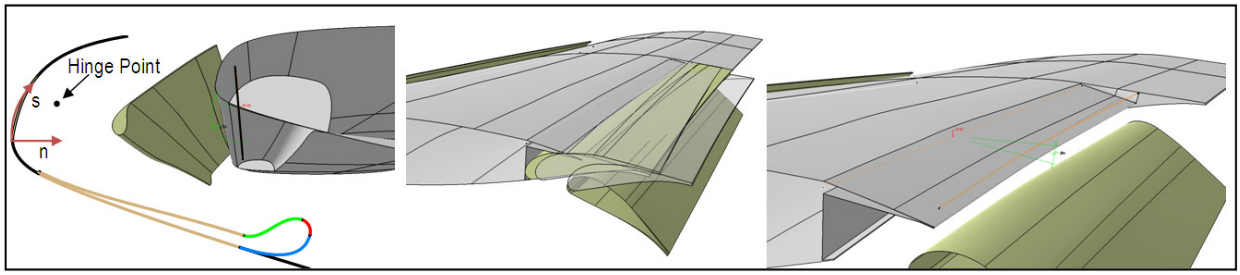

Figure 21: Setting modifications of high-lift devices (Krueger root hinge point coordinates and device deflection: 3 parameters – Fowler flap full 3D deployment: 5 parameters – spoiler deflection: 1 parameter).

According to the studies performed in §3.4, constraints to the Krueger hinge line position were introduced due to space allocation issues for a feasible actuation system and to avoid part clash during rotation. Restrictions to the Krueger extended position were also introduced to comply with minimum shielding requirements prescribed by the industry to protect the main wing leading edge by insect contamination. All these constraints were tested after any geometry update in a CAD-in-the-loop optimization process. Steady RANS simulations were performed using a parametric CFD model of the wing alone, consisting of a multi-block structured hexahedral mesh (4.3M cells, shown in Figure 22) and a topology update script to fit the grid blocking onto the modified geometry. The computational domain was extended about 20 chords ahead and behind the wing in the streamwise direction, 10 chords above and below, and 5 half-spans in the lateral direction. Each flow simulation was run as a restart from the baseline solution and the boundary layer was solved down to the wall around all solid boundaries using the k-ω SST turbulence model. A preliminary (human driven) design stage, based on trial and error approach, allowed to define with a limited effort a reference baseline configuration matching the target $C_{L,\max}$ (2.63 with 5° spoiler deflection), as well as all other constraints and requirements. Single-Objective Genetic Algorithm optimizations were then run combining the two design objectives (at DP1 and DP2, Table 3) into their weighted sum and introducing a quadratic penalty to account for $C_{L,\max}$ constraint violations.

$$f_{obj} = \underbrace{w_1 \cdot C_L\big|_{DP1}}_{OBJ_1} + \underbrace{w_2 \cdot \left(E^2 C_L\right)\Big|_{DP2}}_{OBJ_2} + \underbrace{w_o \cdot \max\left(0, sign\left(2.54 - C_L\right) \cdot \left(C_L - 2.54\right)^2\right)\Big|_{DP0}}_{\text{Quadratic Penalty}} \quad (1)$$

Due to computational resources and time constraints, the angle of attack at DP0 was frozen during the optimization loop at the value corresponding to C_L=$C_{L,\text{TARGET}}$=2.54 for the baseline configuration, without searching for maximum lift point at every configuration update.

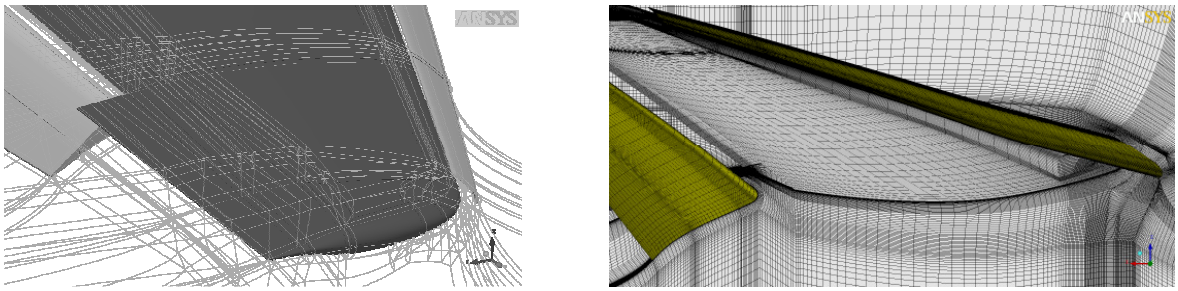

Figure 22: Grid topology and mesh size overview.

A genetic algorithm developed at CIRA was used for the numerical optimization task. Initially, the weights values were determined in such a way that a 1% variation of either OBJ_1, OBJ_2 or $C_{L,DP0}$ produced an equal percentage variation of the cumulative objective, which value was set to -1 for the baseline configuration. A population of 36 individual evolved for 16 generations during a preliminary explorative GA run, using a standard random initialization around the baseline, 100% crossover and 3% mutation probabilities. Although a reduction of about 8.5% was obtained for the cumulative objective (black dots, Figure 23), opposite trends were observed in the evolution of the two objective components, achieving a 30% improvement on OBJ_1 but with a performance degradation of about 13% in the aerodynamic efficiency at landing approach (OBJ_2), which improvement was the intended goal of the design optimization. Therefore a second GA run (13 additional generations) was performed using an OBJ_2 weight value amplified by a factor of 4 (red dots, Figure 23) and including inside the initial population a collection of individuals randomly selected from the first GA run evolution. This was sufficient to drive the design towards improved landing performance (ΔOBJ_2=-2.5%) and a post design check on the optimized configuration verified that the predicted maximum lift coefficient is 2.63 (as for the baseline configuration), sufficiently above the specified target. A wing lift loss due to the separation of its outermost sections (not equipped with any HL device) is observed for both the baseline and the optimized designs, and produces the lift slope reduction observed in Figure 23 (upper right plot). Flow visualizations highlighted that a reattachment occurs on that area at higher angles of attack due to increased downwash from the tip vortex, and finally the wing stall is triggered by Krueger separation starting at about 20% of the half-span, with attached flow observed over the whole flap surface up to 2° beyond maximum lift incidence, where the predicted wing lift capability reduces to 50% of the maximum. Despite a desired optimum location should fall in the grey area of Figure 23, where both of the objectives are improved, the slight decreases in the lift coefficient at DP1 do not represent an issue for the design, as no significant flow separation appeared at V_{FE^*} for the selected optimal configuration (upper right area, Figure 23) that was the intended scope of OBJ_1. The drag saving at landing approach (C_L=1.68) is 18 counts compared to the baseline design, and is almost equally distributed between induced and parasite components. A total of 96 CPU cores were dedicated to each CFD run on a remote supercomputing facility. The

evaluation of each individual over all the DPs required approximately 70 minutes leading to 42 hours elapsed to complete each generation running the GA optimizer in serial mode. Finally, in Figure 24 it is shown a comparison of optimized versus baseline HL configurations at the wing root section. An increase of downward spoiler deflection revealed beneficial to the design and the optimal setting (~7.4 degrees) did not exceed the maximum allowed deflection of 8 degrees suggested by the industry.

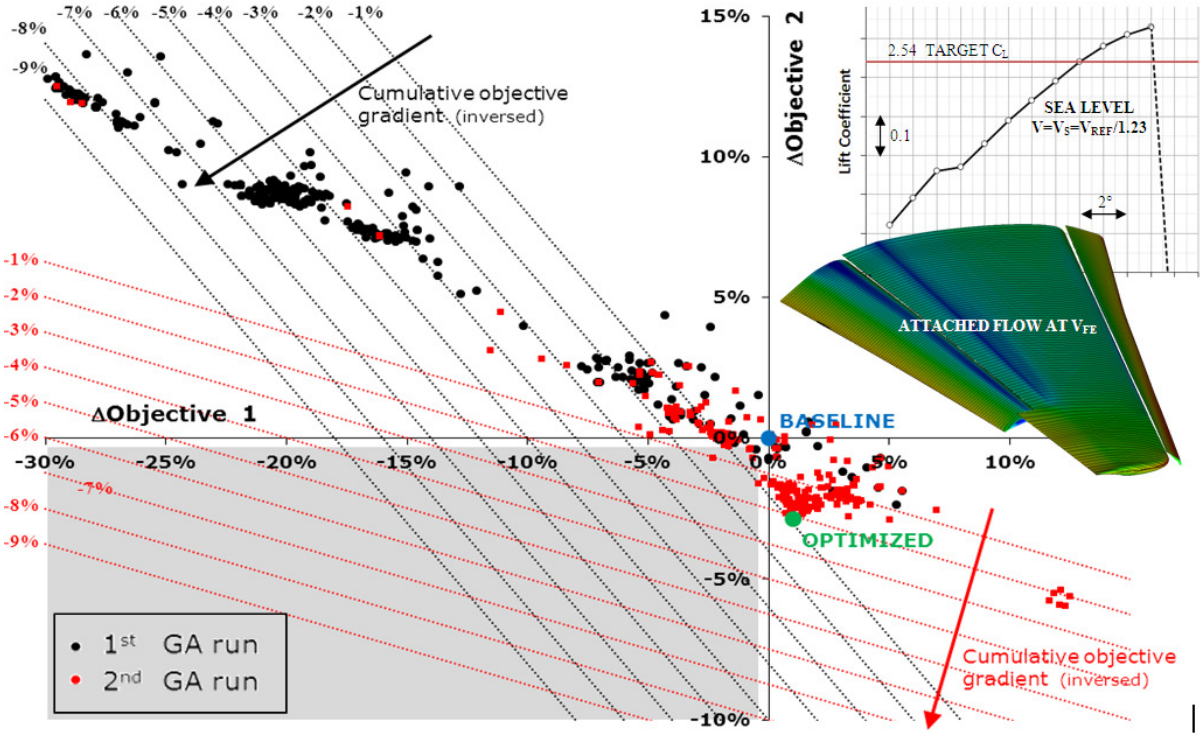

Figure 23: Optimizations evolution in the objectives space, lift curve (at DP0) and skin friction streamtraces (at DP1) for the optimal configuration.

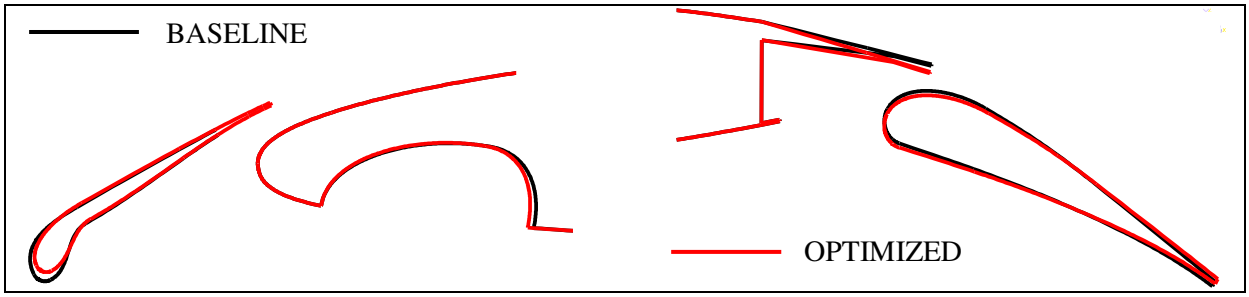

Figure 24: Baseline vs. Optimized HL configurations at wing root section.

4 CONCLUSIONS

The design and optimization of a high lift system for a High Aspect Ratio Low Sweep wing featuring Natural Laminar Flow at transonic cruise conditions is targeted in the DeSiReH project. Within this paper two main areas of investigation have been described, both dedicated to the application of CFD-based automatic optimization tools currently available and applied within the aerospace community for HL design purposes.

The first area of investigation was devoted to the analysis of concurrent optimization strategies, by considering a complex realistic problem for a classical three element HL system optimization. Based on the information gathered from the different partners' approaches, it was

possible to draw up some general guidelines and suggested areas for future investigations. The first outcome of this study is that the employment of automatic optimization in HL design can provide larger improvements (a factor of 2) compared to current industrial approaches based on "by hand" optimization requiring high human interaction and expertise. On the other hand, the investigations carried out have also revealed that in automatic optimization even an inadequate exploration of the design space (*e.g.*, due to the usage of a large number of design variables) can produce at least comparable results to what is obtainable with the above industrial approach. In this context, the usage of meta-models can improve automatic optimization tools in the sense of a faster and wider exploration of large design spaces or, on the other hand, a simplification of the problem wherever sequentialization/decoupling strategies are applicable. As observed, not all the strategies aimed at reducing the design space are effective and suitable strategies must be assessed *a-priori* by preliminary analyses or pre-knowledge of the HL optimization problem. With reference to this, the employment of "engineering-knowledge" optimization strategies based on the observation of suitable physical sensors has proven to be very powerful and cost-effective. Finally, the coupling of a research-developed optimization software with currently available industrial CFD tools revealed to be successful and feasible in performing a fully automatic 3D HL optimization of industrial interest.

The experience gained in the first part of the DeSiReH project was exploited in a second phase, wherein the design of a HL system was carried for a future transport aircraft adopting a HARLS wing featuring NLF at transonic cruise conditions. In a first exploratory phase several leading edge HL concepts (*i.e.* the slotted Krueger, the Large Slat and the Drooped Nose) have been pre-optimized to achieve a target $C_{L,\max}$ without including feasibility constraints. The slotted Krueger concept was down-selected, according to the achieved performance in terms of $C_{L,\max}$, drag, impact on laminarity and leading edge insect shielding properties. Then, three different designs have been generated for the selected slotted Krueger+Fowler flap system: one design is based on standard procedures used in industry (driven by high-lift aerodynamics expertise) and two other designs were carried out by using automatic numerical optimization working with different formulations of the problem. Between these last two designs, one was selected (according to aerodynamic criteria based on $C_{L,\max}$, $\alpha_{\max}$, C_D, C_L behavior in the full flight envelope) to generate an initial 3D wing HL model, to be further optimized by means of the 3D CFD optimization tools settled up in the first part of the project. During this phase, several kinematics, mechanical integration feasibility and structural sizing studies have been conducted by also exploiting the CFD generated aerodynamic data, in order to continuously supply the optimizing partners with as much as possible realistic constraints. The final part of the design phase was then dedicated to the 3D automatic optimization with all the constraints included and aimed at improving the aerodynamic efficiency at landing and approach conditions, while preserving attached flow on the flap over the complete speed range and providing a $C_{L,\max}$ above a specified target. The 3D optimization work required an intensive usage of computational resources which anyway seem to be of affordable level for the aerospace industry nowadays or in the near future.

In the following of the DeSiReH project the developed 3D high-lift models based on both industrial expertise and automatic optimization, respectively, will be tested in the European Transonic Wind Tunnel at low-speed and flight Reynolds numbers. This experimental campaign will be used to assess the predicted aerodynamic performance of the designed HL systems and to quantify, in a realistic framework, the added value of using automatic CFD optimization to design aircraft high-lift devices.

ACKNOWLEDGEMENT

This work has been performed within the scope of the DESIREH project funded by the European 7th Framework Programme under grant number ACP8-GA-2009-233607. Special thanks to the consortium of the European 7th Framework Programme TELFONA, especially David Sawyers, Airbus UK, for providing the laminar clean wing shape for the investigations within this project. The authors are also grateful to Henning Strueber, Airbus-Germany, for providing a continuous industrial feedback to the HARLS wing HL optimization working group and to Domenico Quagliarella, CIRA, who was strongly involved in the integration of the CIRA in house developed GA optimizer with Piaggio Aero Industries CAE tools.

REFERENCES

[1] European Commission: "Aeronautics and Air Transport Research - 7th Framework Programme 2007-2013", European Union, ISBN 978-92-79-14287-1 (2012), pp. 34-36.

[2] J. Ponsin, M. Meheut: Comparison of Grid Adaptation Techniques for High-Lift Flow Applications. *ECCOMAS 2012 Conference, Aeronautics Special Technology Session, STS01: Progress in CFD for High-Lift Application and Design.*

[3] P. Eliasson, C. Marongiu, S. Bosnyakov: Acceleration of URANS for application to separated high-lift flows. *ECCOMAS 2012 Conference, Aeronautics Special Technology Session, STS01: Progress in CFD for High-Lift Application and Design.*

[4] P. Iannelli, D. Quagliarella: Multi-objective/Multi-point shape and setting high-lift system optimization by means of genetic algorithm and 2D Navier-Stokes equations. *EUROGEN 2011 Conference proceedings, Capua, Italy*.

[5] M. Minervino, P. Iannelli, D. Quagliarella: 3D Flap design using Navier-Stokes equations and evolutionary optimization techniques on an industrial platform. *EUROGEN 2011 Conference proceedings, Capua, Italy*.

[6] E. Benini, R.Ponza, P. Iannelli, H. Strüber, Z. Hrncir, F. Moens and T. Kuehn: Multi-point shape and setting optimization of high-lift airfoils in both take-off and landing conditions. *ECCOMAS 2012 Conference proceedings, TO-28*, *Vienna, Austria.*

[7] J. Wild, J. Brezillon, O. Amoignon, J. Quest, F. Moens, D. Quagliarella: Advanced design by numerical methods and wind-tunnel verification within European high-lift program. *Journal of Aircraft, Vol. 46, No. 1, January–February 2009.*

[8] F. Moens, C. Wervaecke: Multi-point optimization of shapes and settings of high-lift system by means of evolutionary algorithm and Navier-Stokes equations. Submitted to *Journal of Engineering Computations*, *Special Issue on Computational Methods in Engineering Design and Optimization,* 2012.

[9] A.M.O. Smith: High-Lift Aerodynamics. *Journal of Aircraft.* Vol. 12, N^{o}6, June 1975.

[10] P.K.C. Rudolph: High-Lift Systems on Commercial Subsonic Airliners. *NASA CR4746*, September 1996.